

Effect of Li-Substitution on the Resistivity and Magnetoresistance of LaMnO_y

A.M. Ahmed · A.K. Diab · H.F. Mohamed

Received: 12 September 2010 / Accepted: 14 September 2010 / Published online: 8 October 2010
© Springer Science+Business Media, LLC 2010

Abstract The temperature dependence of the resistivity (ρ) and magneto-resistance (MR) effect of $\text{La}_{1-x}\text{Li}_x\text{MnO}_y$ ($x = 0.05, 0.1, 0.15, 0.2 \& 0.25$ at.%) fixed valence doped compounds were studied between 80 and 320 K. X-ray powder diffraction (XRD) at room temperature shows that the samples are single phase. The resistivity of all samples with and without magnetic field shows a metal–semiconductor (M–S) transition for all compositions. In addition, the replacement of the Li-substitution results in a reduction of the transition temperature T_{ms} and increases ρ . In the magnetic field of 0.5 Tesla a large negative magnetoresistance (MR = 50%) was observed, which is encouraging for potential application of colossal magnetoresistance (CMR) material at low fields. We determine the activation energy (E_ρ) in the semiconductor region.

Keywords The resistivity · Colossal magnetoresistance · Curie temperature

1 Introduction

The discovery of colossal magnetoresistance (CMR) in perovskite manganites $\text{Ln}_{1-x}\text{A}_x\text{MnO}_3$ (Ln is a trivalent rare-earth ion and A is a divalent alkaline-earth-metal ion) has attracted considerable scientific and technological interest due to their exotic electrical and magnetic properties [1, 2]. Most of these interesting physical properties of the manganites are correlated with the

double-exchange (DE) mechanism [3, 4], i.e. the hopping of e_g electrons between spin-aligned Mn^{3+} and Mn^{4+} ions through oxygen ions. Recently, a number of groups [5, 6] have presented arguments to show that the double-exchange model alone is not sufficient to explain the CMR effect of the manganites. They suggested that a strong spin–phonon interaction arises from the Jahn–Teller effect (deformation of the Mn^{+3}O_6 octahedra) in conjunction with the spin-electron-phonon interaction triangle, which is typical for manganites and plays an important role in the localization of carriers and origin of CMR. The lattice distortion not only influences the effective transfer integral of e_g electrons but also the superexchange interaction between manganese ions, as well as the magnetic structure of the compounds. Different local distortions of the lattice around different ions could result in magnetic inhomogeneity in the compounds and give rise to an intriguing magnetic structure and MR behavior [7]. One of the main features of doped rare-earth manganites is the electronic phase separation [8] scenario. This separation into insulating superexchange coupled and metallic double-exchange coupled phase segments occurs predominantly below the Curie temperature T_C , which might explain the complicated and fascinating CMR behavior well below and above the Curie temperature, T_C . So far, most studies have focused on the divalent alkaline-earth-metal doping in $\text{Ln}_{1-x}\text{A}_x\text{MnO}_3$ compounds. In contrast, there are few reports on the study of monovalent alkaline-metal-doped samples [9–17]. Due to the differences in valence, alkaline-earth-metal doping and alkali-metal doping in LaMnO_3 can result in remarkably different consequences. In particular, it was reported that $\text{Ln}_{1-x}\text{A}_x\text{MnO}_3$ (A = Na, K, Li and Rb) compounds crystallize in a rhombohedrally distorted perovskite structure without static Jahn–Teller deformation (space group R3-c) [18].

A.M. Ahmed (✉) · A.K. Diab · H.F. Mohamed
Physics Department, Faculty of Science, Sohag University,
82524, Sohag, Egypt
e-mail: Fikry_99@yahoo.com

Therefore, the study of alkali-metal doping will offer a complementary understanding on the structure and electronic transport of doped LaMnO_3 crystals, which is significant for achieving a complete understanding of the CMR effect in distorted perovskite manganites. Specifically, in this manuscript, we report here the effect of the lithium substitution on the physical properties of samples.

2 Experimental

The polycrystalline $\text{La}_{1-x}\text{Li}_x\text{MnO}_y$ samples ($x = 0.05, 0.1, 0.15, 0.2$ and 0.25 at.%) have been prepared by standard solid-state reaction method; stoichiometric amounts of La_2O_3 , Li_2CO_3 and MnCO_3 powders (all having 99.99% purity) were thoroughly mixed and grinding. After grinding, the powders were pressed into pellets with a pressure of 2 ton/cm² and calcined at 1273 K for 15 h. Followed by cooling to room temperature, they were reground and again pressed into pellets with a pressure of 7 ton/cm² and subsequently annealed at 1373 K for 10 h. The samples were examined by X-ray powder diffraction analysis, which indicated the presence of single phase with perovskite-type structure. The XRD analysis was performed using Brucker (Axs-D8Advance) diffractometer at room temperature with $\text{CuK}\alpha$ radiation ($\lambda = 1.5406 \text{ \AA}$). The resistivity was measured as a function of temperature using the standard four-probe method and air-drying conducting silver paste as in previous works [16, 17, 19]. The magnetoresistance (MR) ratio is defined by $\text{MR} = \delta\rho/\rho_0 = (\rho_H - \rho_0)/\rho_0$, where ρ_H and ρ_0 are resistivities with and without an applied magnetic field (0.5 T), respectively.

3 Results and Discussion

Figure 1 shows powder X-ray diffraction patterns of the polycrystalline $\text{La}_{1-x}\text{Li}_x\text{MnO}_y$ samples ($x = 0.05, 0.1, 0.15, 0.2$ & 0.25 at.%). The XRD patterns of samples reveal that the prepared samples have a single-phase rhombohedral structure with a space group R3-c (this results agree with Shimura [18] and Wang et al. [20]). In general, all the peaks of five samples satisfy the La–Li–Mn–O phase. The structural parameters are refined by the standard Rietveld technique [21]. The lattice volume, lattice distortion and the bond lengths (Mn–O) decrease with increasing Li-substitution [22]. It is well known that one of the possible origins of the lattice distortion of perovskite-based structures is the deformation of the MnO_6 octahedra originating from Jahn–Teller (JT) effect that is inherent to the high-spin ($S = 2$) Mn^{3+} ions with double degeneracy of the e_g orbital. Obviously, this kind of distortion is directly related

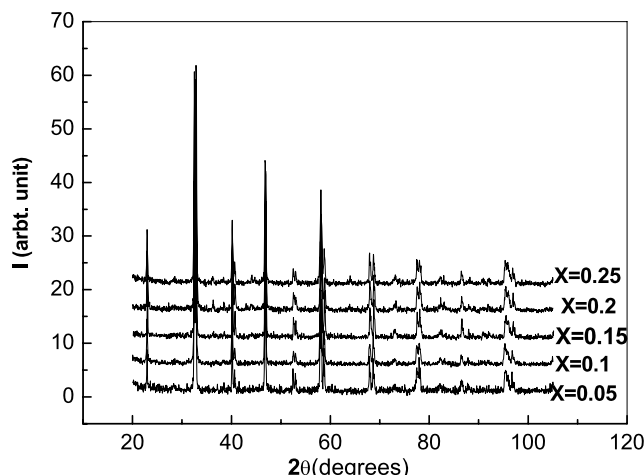


Fig. 1 X-ray diffraction patterns of $\text{La}_{1-x}\text{Li}_x\text{MnO}_y$

to the concentration of Mn^{3+} ions. Another possible origin of the lattice distortion is the average ionic radius of the A-site element, which is related to the tolerance factor t [$t = (r_A + r_o)/\sqrt{(r_B + r_o)}$], where r_A , r_B and r_o radius of A cation, B cation and oxygen element. As t is close to 1, the cubic perovskite structure is realized. As r_A decreases, so does t , and the lattice structure transforms to the rhombohedral ($0.96 < t < 1$) and then to the orthorhombic structure ($t < 0.96$), in which the bending of B–O–B bond increase and the bond angle deviates from 180°. For LaLiMnO_3 samples, we think that the room-temperature structural transformation originates mainly from the variation of the tolerance factor t induced by the partial substitution of smaller Li^{1+} ($r = 0.76 \text{ \AA}$) ions for large La^{3+} ions ($r = 1.032 \text{ \AA}$). This results agree with Ye et al. [22]. The reverse lattice distortion from orthorhombic to rhombohedral symmetry due to larger Sr^{3+} ions partially substituting for La^{3+} ions has been observed $\text{La}_{1-x}\text{Sr}_x\text{MnO}_3$ compounds [23, 24].

Figure 2 shows the variation of resistivity with temperature for $\text{La}_{1-x}\text{Li}_x\text{MnO}_y$. Obviously, the resistivity increases with Li doping. We expect that when the Li-content increases not only the La-content decreases but also the charge carrier density [25], which leads to a reduction of the double exchange which is proportional to bandwidth. Therefore, the La/Li configuration plays a prominent role in controlling the resistivity. Consistently, the figure shows that the transition temperature (M–S) for LaLiMnO_y decreases with the increase of Li. These compounds have a distinct metallic phase below the transition temperature (T_{ms}), and above this temperature they become semiconducting.

The equilibrium metal-insulator transition temperature might be T_{ms} or the small structure found on the ascending slope of Fig. 3a, b. However, both go to low temperatures with increasing Li doping. The inset of Fig. 2 reveals that T_{ms} moves to lower temperatures with the increment of the lithium concentration. The lithium will alter the

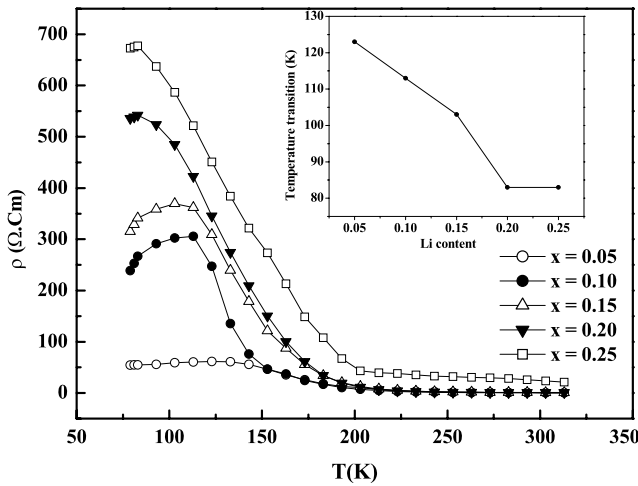


Fig. 2 The resistivity versus temperature for $\text{La}_{1-x}\text{Li}_x\text{MnO}_y$ the inset shows the composition dependence of the temperature transition (T_{ms})

$\text{Mn}^{4+}/\text{Mn}^{3+}$ ratio, which is one of the factors which determine the transport and magnetic properties of samples. In addition a decrease in T_{ms} with increasing Li-content can be interpreted as an increasing strength of the Mn–O–Mn bond with decreasing average A site ionic radius $\langle r_A \rangle$ due to the partial substitution of smaller Li^{1+} ions for larger La^{3+} ions. This substitution causes a narrowing of the bandwidth and thus decreasing of e_g electrons, which in turn results in a weakening of the double-exchange mechanism via the bandwidth b [26].

The conduction above the insulator–metal transition temperature (T_{ms}) is still a matter of controversy as numerous groups have reported different behavior. Some of these groups find that the mechanism of conduction above T_{ms} is an extended state [27, 28]. In this case, the dependence of σ on T can be represented by the well-known Arrhenius formula:

$$\rho = \rho_0 \exp(E_\rho/k_B T) \quad (1)$$

where σ_0 is the pre-exponential factor (which includes the carrier mobility and density of states), E_ρ is the corresponding activation energy of electrical conductivity and k_B is the Boltzmann constant. Others find that Mott's Variable Range Hoping (VRH) expression is appropriate [29, 30].

$$\rho = \rho_0 \exp\left[\left(\frac{T_0}{T}\right)^{1/4}\right], \quad (2)$$

$$T_0 = 16[\alpha^3/k_B N(E_F)] \quad (3)$$

where ρ_0 is a pre-exponential factor, α is the coefficient of exponential decay of the localized state wave function, which assumed to be 0.124 \AA^{-1} and $N(E_F)$ is the density of localized states (DOLS) at the Fermi level.

Table 1 Variations of E_ρ (eV) and σ_0 ($\Omega^{-1} \text{ cm}^{-1}$) as functions of compositions for $\text{La}_{1-x}\text{Li}_x\text{MnO}_y$ system (high range T)

X	E_ρ (eV)	ρ_0 ($\Omega \text{ cm}$)
0.05	0.1711	1295.562
0.1	0.1654	1885.975
0.15	0.1512	493.045
0.2	0.1303	223.247
0.25	0.0318	7.229

Table 2 Variations of $N(E_F)$ ($\text{cm}^{-3} \text{ eV}^{-1}$), N (cm^{-3}) and ρ_{02} ($\Omega \text{ cm K}^{1/2}$) as functions of compositions for $\text{La}_{1-x}\text{Li}_x\text{MnO}_y$ system (above T_m)

X	$N(E_F) \text{ eV}^{-1} \text{ cm}^{-3}$	$N = 2k_B T N(E_F) (\text{cm}^{-3})$	$\rho_{02} (\Omega \text{ cm K}^{1/2})$
0.05	4.750 E^{18}	2.456 E^{17}	3.470 E^{-07}
0.1	1.751 E^{18}	9.054 E^{16}	1.990 E^{-09}
0.15	1.094 E^{18}	5.657 E^{16}	2.418 E^{-10}
0.2	7.487 E^{17}	3.871 E^{16}	1.951 E^{-11}
0.25	5.357 E^{17}	2.770 E^{16}	1.470 E^{-12}

Because we have a divided resistivity above T_{ms} , we discuss both parts separately. One part (the higher temperatures) is close to an Arrhenius law, the other is closer to a Mott law (VRH). So we did further reduce the data according to these two models without claiming to understand completely the underlying transport mechanism.

Using (1), we calculated E_ρ in the high range of T and tabulated the results in Table 1. It is obvious that both the values of E_ρ and σ_0 decrease with increasing Li-content; this shows that the thermal activity of LaLiMnO composition increases with increasing Li-content. The larger values of E_ρ (see Table 1) agree with previous work [27, 28]. The values of E_ρ change from 0.032 to 0.171 eV.

The Mott parameters of variable range hopping conduction, namely, the density of localized states (DOLS) at the Fermi level, $N(E_F)$, are calculated from the slopes above T_m . The concentration of conduction electrons (N) within a range of $k_B T$ of the Fermi energy can be calculated using $2k_B T N(E_F)$. The compositional dependencies of $N(E_F)$, N , are calculated and recorded in Table 2. The obtained $N(E_F)$ and N data are decreased with the investigated compositions. On the other side, the values of ρ_{02} were decreased with increasing Li-content. The charge carrier concentration (N) decreases with increasing Li concentration in $\text{La}_{1-x}\text{Li}_x\text{MnO}_y$, confirming the observed increase in resistivity as due to a decrease in carriers with Li substitution.

The temperature dependences of the resistivity in zero applied field (ρ_0) and at 0.5 T ($\rho_{0.5\text{T}}$) of the five samples are shown in Fig. 3. The resistivity shows a semiconducting

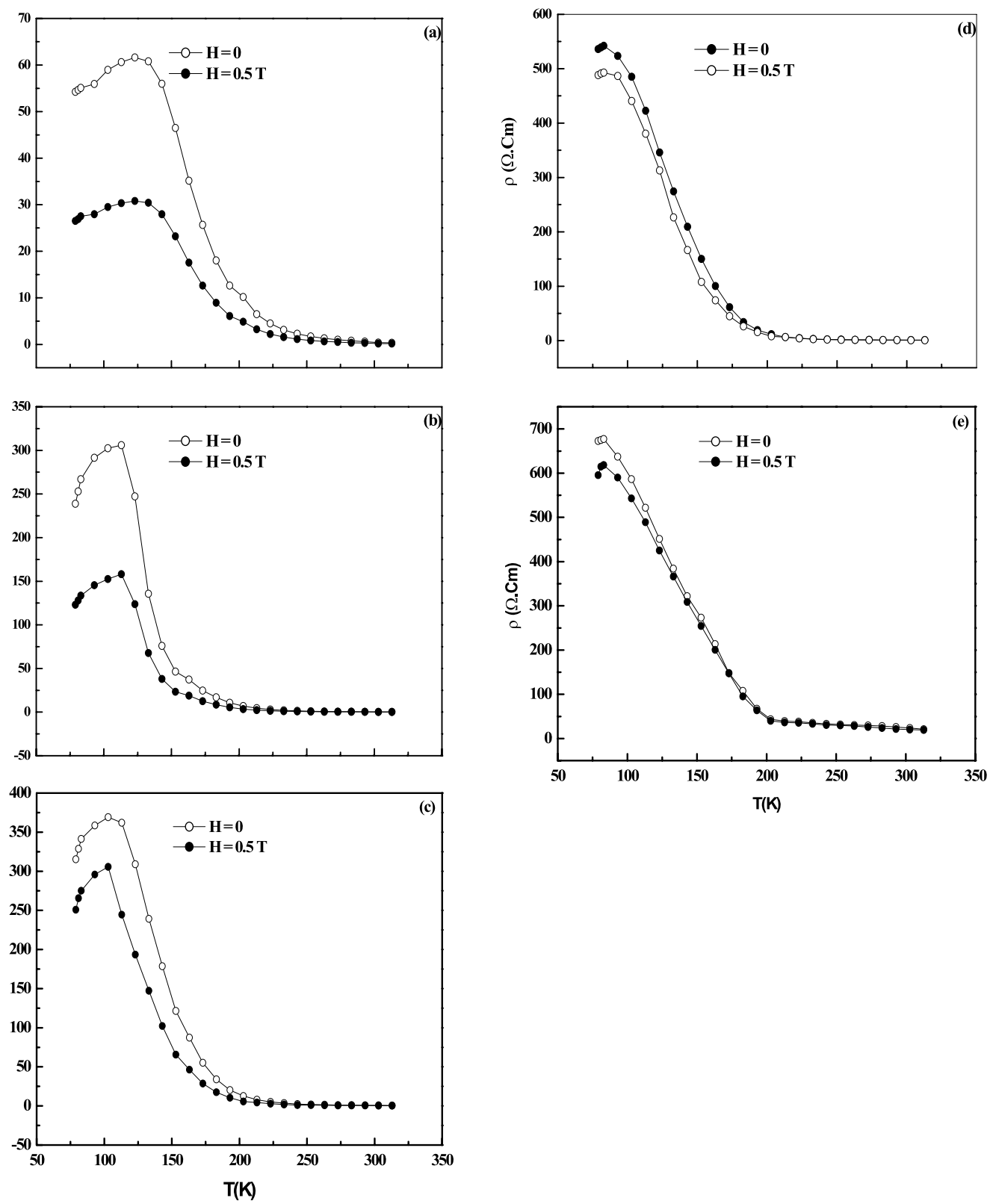


Fig. 3 The variation of resistivity in zero magnetic field and $H = 0.50 \text{ T}$ with respect to temperature for Li content of $\text{La}_{1-x}\text{Li}_x\text{MnO}_y$ where $a - x = 0.05$, $b - x = 0.1$, $c - x = 0.15$, $d - x = 0.2$ and $e - x = 0.25$ at.%

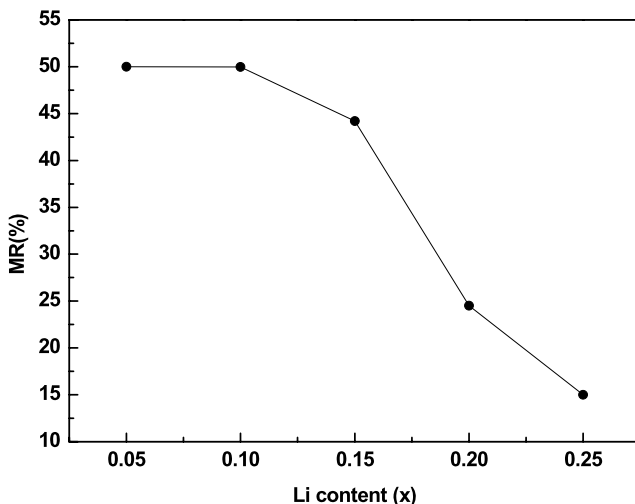


Fig. 4 Li doping level dependence of room temperature MR of $\text{La}_{1-x}\text{Li}_x\text{MnO}_y$ at magnetic field 0.5 T

behavior above the metal-semiconductor transition temperature (T_{ms}) for all cases. An applied magnetic field of 0.5 T suppresses the resistivity, giving a large negative magnetoresistance. The resistivity at T_{ms} decreases with the highest value, this shows a high magnetoresistance (MR) at T_{ms} and below it. As shown in Fig. 4, the MR decreases with increasing the level of doping Li at room temperature. The value of MR reaches 50% at room temperature especially for low content of Li, which is encouraging for potential application of colossal magnetoresistance (CMR) material at low fields. As mentioned before, above T_{ms} the resistivity is much activated as function of T , it changes from a fraction of $\Omega\text{-cm}$ to 500 $\Omega\text{ cm}$ for samples rich with Li-content. Therefore, it is observed that the values of MR are approximately of the whole range of T for every sample.

The negative magnetoresistance MR% defined as:

$$\text{MR} = (\rho_H - \rho_0)/\rho_0 \quad (4)$$

4 Conclusion

Electrical resistivity and magnetoresistance of monovalent alkali metal (Li) substituted LaMnO_3 polycrystalline pellets prepared by solid-state reaction procedure have been studied between 80 and 320 K. X-ray diffraction patterns showed a single-phase rhombohedral structure of all samples. The resistivity versus temperature shows a metal–semiconductor transition for all samples. The M–S transition temperature decreases with increasing Li-content. This is due to the partial substitution of smaller Li^{1+} ions for larger La^{3+} ions or due to Zener bond blocking.

The MR ratio of the LaLiMnO_y is about 50% under a low field ($H = 0.5$ tesla) for low doping Li-content. This

result opens new opportunities to improve the performance of colossal magnetoresistive devices.

Acknowledgements The authors would like to thank Abd El Mo'ez A. Mohamed and Sara Abo El-Hassan for their help in the preparation of the samples.

References

1. von Helmolt, R., Wecker, J., Holzapfel, B., Schultz, L., Samwer, K.: Phys. Rev. Lett. **71**, 2331 (1993)
2. Imada, M., Fujimori, A., Tokura, Y.: Rev. Mod. Phys. **70**, 1039 (1998)
3. Zener, C.: Phys. Rev. **82**, 403 (1951)
4. de Gennes, P.G.: Phys. Rev. **118**, 141 (1960)
5. Millis, A.J., Littlewood, P.B., Shraiman, B.I.: Phys. Rev. Lett. **74**, 5144 (1995)
6. Alexandrov, A.S., Bratkovsky, A.M.: Phys. Rev. Lett. **82**, 141 (1999)
7. Rao, G.H., Sun, J.R., Liang, J.K., Zhou, W.Y.: Phys. Rev. B **55**, 3742 (1997)
8. Uehara, M., Mori, S., Chen, C.H., Cheong, S.-W.: Nature (Lond.) **399**, 560 (1999)
9. Das, S., Dey, T.K.: Solid State Commun. **134**, 837 (2005)
10. Das, S., Dey, T.K.: Physica B **381**, 280 (2006)
11. Li, Z.Q., Jiang, E.Y., Zhang, D.X., Hou, D.L., Li, W.C., Bai, H.L.: Phys. Lett. A **277**, 56 (2000)
12. Roy, S., Guo, Y.Q., Venkatesh, S., Ali, N.: J. Phys. Condens. Matter **13**, 9547 (2001)
13. Das, A., Sahana, M., Yusuf, S.M., Medhav Rao, L., Shivakumara, C., Hegde, M.S.: Mater. Res. Bull. **35**, 651 (2000)
14. Shivakumara, C., Subbana, G.N., Lalla, N.P., Hegde, M.S.: Mater. Res. Bull. **39**, 71 (2004)
15. Das, S., Dey, T.K.: J. Magn. Magn. Mater. **311**, 714 (2007)
16. Ahmed, A.M., Saleh, S.A., Ibrahim, E.M.M., Bontempib, E., Mohamed, H.F.: J. Magn. Magn. Mater. **320**, L43 (2008)
17. Ahmed, A.M., Saleh, S.A., Ibrahim, E.M.M., Mohamed, H.F.: J. Magn. Magn. Mater. **301**, 452 (2006)
18. Shimura, T., Hayashi, T., Inaguma, Y., Itoh, M.: J. Solid State Chem. **124**, 250 (1996)
19. Ahmed, A.M.: Physica B **352**, 330 (2004)
20. Wang, X.L., Kennedy, S.J., Gehringer, P., Liu, H.K., Lang, W., Dou, S.X.: J. Appl. Phys. **83**(11), 7177 (1998)
21. Wiles, D.B., Young, R.A.: J. Appl. Crystallogr. **14**, 149 (1981)
22. Ye, S.L., Song, W.H., Dai, J.M., Wang, S.G., Wang, K.Y., Yuan, C.L., Sun, Y.P.: J. Appl. Phys. **88**(10), 5915 (2000)
23. Urushibara, A., Moritomo, Y., Arima, T., Asamitsu, A., Kido, G., Tokuro, Y.: Phys. Rev. B **51**, 14103 (1995)
24. Mitchell, J.F., Argyriou, D.N., Potter, C.D., Hinks, D.G., Jorgensen, J.D., Bader, S.D.: Phys. Rev. B **54**, 6172 (1996)
25. Rao, G.H., Sun, J.R., Kattwinkel, A., Haupt, L., Bärner, K., Schmitt, E., Gmelinn, E.: Physica B **269**, 379 (1999)
26. Hwang, H.Y., Cheong, S.-W., Radaelli, P.G., Marezio, M., Battlogg, B.: Phys. Rev. Lett. **75**, 914 (1995)
27. Xiong, G.C., Bhagat, S., Li, Q., Dominguez, M., Ju, H., Greene, R., Venkatesan, T.: Solid State Commun. **97**, 599 (1996)
28. Hundley, M.F., Hawley, M., Heffner, R.H., Jia, Q.X., Neumeier, J.J., Tesmer, J.: Appl. Phys. Lett. **67**, 860 (1995)
29. Coey, J.M.D., Viret, M., Ranno, L., Ounadjela, K.: Phys. Rev. Lett. **75**, 3910 (1995)
30. Viret, M., Ranno, L., Coey, J.M.D.: Phys. Rev. B **55**, 8067 (1997)